Available online at www.sciencedirect.com
SCIENCE DIRECT®
Pergamon
Acta Materialia 51 (2003) 4095–4105
Acta MATERIALIA
www.actamat-journals.com

The effect of compression and tension on shear-band structure and nanocrystallization in amorphous $Al_{90}Fe_5Gd_5$: a high-resolution transmission electron microscopy study

W.H. Jiang [a], M. Atzmon [a,b,*]

[a] *Department of Nuclear Engineering and Radiological Sciences, University of Michigan, 2355 Bonisteel Boulevard, Ann Arbor, MI 48109-2104, USA*

[b] *Department of Materials Science and Engineering, University of Michigan, 2355 Bonisteel Boulevard, Ann Arbor, MI 48109-2104, USA*

Received 31 January 2003; received in revised form 26 March 2003; accepted 22 April 2003

Abstract

Using both conventional and high-resolution transmission electron microscopy (HRTEM), the effect of bending at room temperature on the microstructure of amorphous $Al_{90}Fe_5Gd_5$ was investigated. In the compressive region, nanocrystallites formed at shear bands, along small cracks and at the fracture surface; in the tensile region, nanocrystallites were observed only at the fracture surface. Combining HRTEM with frequency filtering, low-density, nanoscale defects at shear bands were imaged. In the compressive region, both the shear bands and the undeformed matrix contain few defects. In the tensile region, there is a uniform distribution of defects within the shear bands. The preferential precipitation of nanocrystallites in the compressive region is attributed to a kinetic effect due to the uniformly distributed free volume in the shear bands. In contrast, the formation of the nanocrystallites at the fracture surfaces is likely due to adiabatic heating induced by fracture.

Keywords: Metallic glasses; Bending test; High-resolution electron microscopy; Nanocrystalline microstructure; Shear bands

1. Introduction

Newly developed amorphous Al–TM–RE alloys, where TM is a transition metal and RE is yttrium or lanthanides, have higher mechanical strength than crystalline, high strength, Al alloys [1,2]. Well-distributed nanocrystallites in the amorphous matrix, formed by partial crystallization, can strengthen it even further [3–5]. Much work on nanocrystallization at elevated temperatures has been reported [6,7]. Kim et al. [4] found that well-distributed nanocrystalline Al particles formed in the amorphous matrix of an Al–Ni–Fe–Nd alloy during uniaxial tension at elevated temperatures. The resulting ultimate tensile strength was greater than 800 MPa at 580 K, three to four times that of crystalline, high strength, Al alloys.

* Corresponding author. Tel.: +1-734-7646888; fax: +1-734-7634540.
E-mail address: atzmon@umich.edu (M. Atzmon).

1359-6454/03/$30.00
doi:10.1016/S1359-6454(03)00229-5

The authors attributed this result to both dispersion strengthening and enhanced thermal stability at the deformation temperature, caused by depletion of Al in the amorphous matrix due to precipitation. Nanocrystalline/amorphous composites show great promise as key structural materials. Lately, attention has been paid to mechanically induced nanocrystallization, such as by ball milling [8–10], bending [11,12], rolling [13], tension [4,14], nanoindentation [15,16] as well as hydrostatic pressure [17,18]. With the exception of Refs. [17,18], these involve plastic deformation.

Generally, mechanical deformation can drive crystalline solids far from their equilibrium state by introducing structural or chemical defects [19]. Crystalline alloys may lose their long-range order and be amorphized as a result of deformation [20]. Deformation can also assist atomic transport and evolution toward equilibrium [10,21]. The effect of deformation on phase evolution is of practical significance for synthesis of nanocrystalline/amorphous composites, their processing and service. In addition, the mechanisms of atom displacement and formation of crystalline phases under plastic deformation are of significant fundamental interest, and have yet to be conclusively explained.

Chen et al. [11], using transmission electron microscopy (TEM), were the first to report the formation of nanocrystallites at shear bands of Al-based amorphous alloys ($Al_{90}Fe_5Gd_5$, $Al_{90}Fe_5Ce_5$ and $Al_{87}Ni_{8.7}Y_{4.3}$) bent at room temperature. High-energy ball milling was also observed to lead to the formation of nanocrystallites in Al-based amorphous alloys [8]. Recently, Gao et al. [14] observed nanocrystal precipitation in amorphous $Al_{90}Fe_5Gd_5$, within vein protrusion on tensile fracture surfaces and along crack propagation paths, as well as within shear bands resulting from bending.

As of yet, no consensus concerning the microscopic mechanism of mechanically induced nanocrystallization has been reached. It has been argued that a temperature rise may play a crucial role in the formation of nanocrystallites. Csontos and Shiflet [22], using analytical electron microscopy, observed radial diffusion fields of Gd and Fe around nanocrystals in amorphous $Al_{90}Fe_5Gd_5$ bent at room temperature. Based on a comparison with similar diffusion fields for thermal crystallization, they argued that these diffusion fields formed due to a significant temperature increase during mechanical deformation. Indeed, the strain rates for both bending and high-energy ball milling are difficult to control. These may exert highly localized deformation on materials in a very short time. Therefore, it is difficult to rule out a temperature effect on nanocrystallization. Recently, we have combined nanoindentation with TEM to study microstructural evolution of amorphous $Al_{90}Fe_5Gd_5$ at a low strain rate, minimizing a temperature rise during mechanical deformation. We found that mechanical deformation at or near room temperature led to the precipitation of Al-rich nanocrystallites [16]. One expects the temperature and stress state to affect the microscopic details of deformation, and therefore of nanocrystallization. The small sample thickness, and the fact that uniaxial tensile samples typically undergo catastrophic failure, make it very difficult to obtain shear bands under purely compressive or tensile stresses. When a ribbon is bent, the stress ranges from maximum compressive at one surface to maximum tensile at the other. Chen et al. [11] did not address the location of the nanocrystallites within the ribbon. The aim of the present work is to investigate nanostructural features of shear bands, and the formation of nanocrystallites, induced by bending deformation in amorphous $Al_{90}Fe_5Gd_5$, in both the tensile and compressive regions.

Shear bands are the main microstructural effect of plastic deformation in amorphous alloys. Usually, they are identified and characterized morphologically, using a scanning electron microscope (SEM). However, less information is available on their nanoscale structure, the details of which are difficult to detect by TEM. Recently, Miller and Gibson [23] developed a method of characterizing the medium-range atomic structure of amorphous solids. This method includes quantitative analysis of electron images and their Fourier amplitudes, essentially combining small-angle scattering and high-resolution imaging from the same microscopic region. This method allowed the identification of nanometer-scale voids in amorphous silica thin films. Following Miller and Gibson, Li et al. [24] studied shear bands in bulk Zr-based metallic glasses and found that they contained a higher

concentration of nanometer-scale voids than undeformed regions. We note that the authors did not address the nature of the applied stress. An investigation of the structure of shear bands in Al-based amorphous alloys is especially significant in the present context, as the shear bands are preferential sites for formation of nanocrystallites. Therefore, the present work employs high-resolution transmission electron microscopy (HRTEM) to examine nanodefects at shear bands in both the tensile and compressive regions. The results are used to elucidate the mechanism of mechanically-induced nanocrystallization.

2. Experimental details

Ingots with nominal composition $Al_{90}Fe_5Gd_5$ (in atomic %) were prepared by arc melting a mixture of the constituent elements in a purified argon atmosphere. Amorphous ribbons (1 mm $\times$ 0.022 mm) were prepared from the master-alloy ingots using a single-roller melt-spinning apparatus. A Cr-plated copper wheel was employed in an Ar atmosphere at a tangential velocity of 40 m s^{-1}.

X-ray and electron diffraction analyses were employed to confirm the amorphous structure of the as-spun amorphous alloy ribbons. Samples were cut from the ribbons, bent 180° and then straightened to approximately 20° at room temperature (see discussion of the stress state below). The bending was performed by sandwiching samples between glass slides in order to insure the accuracy of the bending angle. A Philips XL30FEG SEM was used to observe shear bands near the bending axis in both the compressive and tensile regions of the bent samples. TEM specimens were prepared electrolytically, using a single-side jet thinning electropolisher in a solution of 25% nitric acid and 75% methanol at 243 K, until a perforation formed. Thinning was performed from one side only, allowing subsequent observation of the region of maximum compression or tension. After jet thinning, the specimens were screened, using an optical microscope, to insure that the perforation was centered near the bending axis. A JEOL 4000EX HRTEM was employed at an operating voltage of 400 kV to observe the deformed regions. The HRTEM images were collected on a charge-coupled device (CCD) camera and their further processing was performed digitally. The instrumental camera length was used for lattice-parameter determination from diffraction patterns. Dark-field images were obtained by displacing the objective aperture so as to minimize the samples' exposure time to the electron beam. We verified that there is no discernible difference between axial and displaced-aperture dark-field images of nanocrystallites.

X-ray diffraction analysis revealed crystallization in cold-rolled ribbon samples, confirming that mechanically induced crystallization was not an artifact due to TEM sample preparation. We performed a set of observations aimed at ruling out an artifact due to atomic displacements or heating by the electron beam in the TEM. We observed no detectable change in the microstructure of shear bands at a magnification of 100 K for exposure to the electron beam up to 30 min. All the results we report were obtained by avoiding placing the focused beam on one sample position for a prolonged time. Conventional TEM observations were generally performed at a magnification around 100 K for less than 5 min. Selected-area electron diffraction (SAED) patterns showing nanocrystallization at shear bands were obtained in 1 or 2 min.

3. Results

As a result of bending and straightening, each side experienced both compression and tension. The side that first underwent compression experienced more compression than tension and vice versa. This has several reasons: (a) Samples were not straightened to 0°. (b) Cracks are observed in both regions already after bending at 90°. Therefore, the initially compressive region experienced little tensile strain during subsequent straightening. (c) The compressive strain is concentrated in a narrow crease, whereas the (limited) compression of the initially tensile region is distributed over a larger volume. Below, we will refer as "compressive" and "tensile" to regions that experienced predominantly one or the other, respectively.

3.1. SEM observation

Fig. 1 displays SEM images of samples bent and subsequently straightened at room temperature. Numerous straight shear bands are observed in both the compressive and tensile regions. These shear bands are unevenly distributed, with their density decreasing with distance from the bending axis. Comparing Fig. 1(a) with Fig. 1(b), it is evident that the density of straight shear bands in the compressive region is lower than that in the tensile region. However, a high density of uneven features, probably also shear bands, is observed in the maximum-strain part of the compressive region. At the same time, cracks can be seen in both regions along the bending axis. Specimens from both the tensile and compressive regions were subsequently observed by TEM.

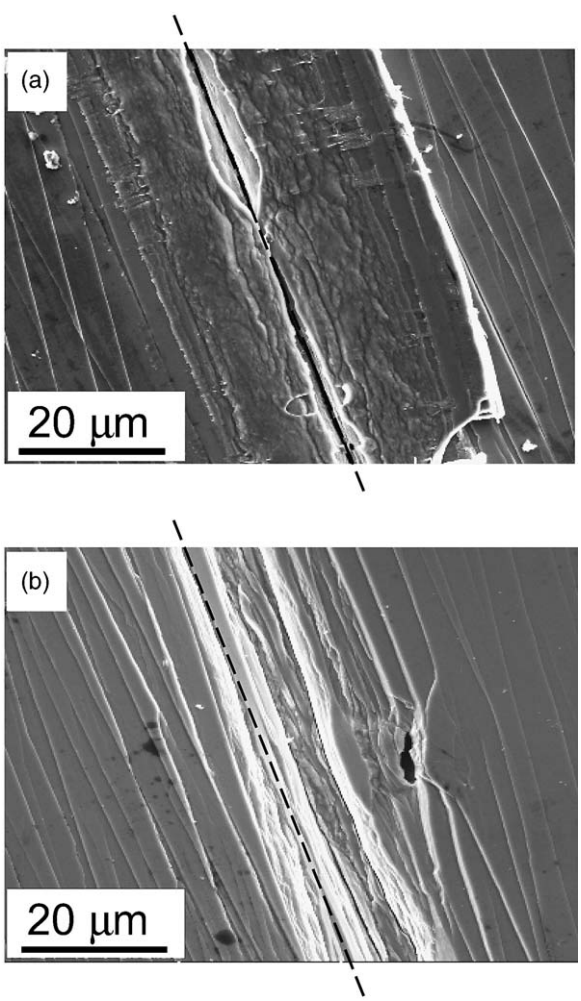

Fig. 1. SEM images of the $Al_{90}Fe_5Gd_5$ bent at room temperature: (a) compressive and (b) tensile region. The lines drawn indicate the bending axis.

3.2. Conventional TEM observation

Consistent with X-ray diffraction result, electron diffraction analysis confirms the amorphous structure of the as-spun amorphous alloy ribbons. Fig. 2 displays a dark-field micrograph of a typical region in the as-received sample, obtained with the first halo ring of the corresponding SAED pattern (inset). No crystalline phase is observed in this sample.

3.2.1. The compressive region

In the compressive region, nanocrystallites are observed at shear bands, small cracks as well as the fracture surface, but not in the undeformed region. An example of nanocrystalline particles at a shear band is shown in a dark-field image in Fig. 3, which also includes the corresponding diffraction pattern. Four sharp diffraction rings are observed, plus diffuse rings originating from the amorphous matrix. The sharp rings were indexed as {111}, {200}, {220} and {311}, respectively,

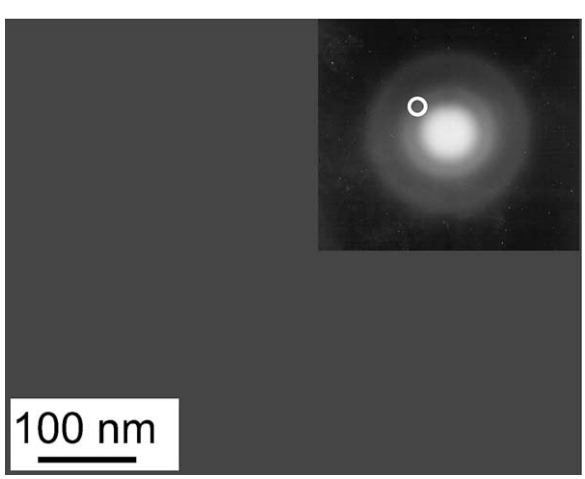

Fig. 2. TEM dark-field image of the as-spun sample. Inset is the SAED pattern, in which the location of the objective aperture is illustrated schematically.

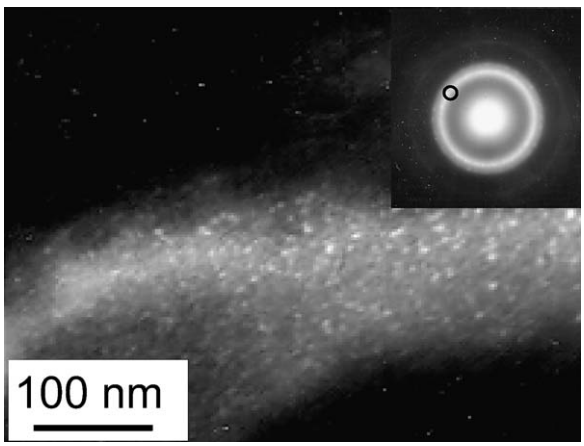

Fig. 3. TEM dark-field image of the compressive region, showing a number of nanocrystallites at a shear band. Inset is its SAED pattern, in which the location of the objective aperture is illustrated schematically.

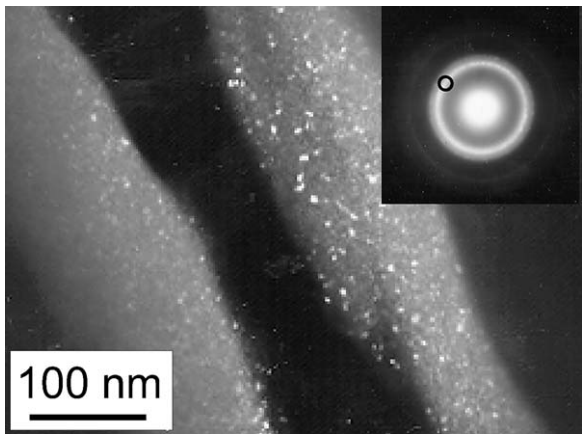

Fig. 4. TEM dark-field image of the fracture surface in the compressive region, showing a number of nanocrystallites. Inset is its SAED pattern, in which the location of the objective aperture is illustrated schematically.

of an fcc phase with a lattice constant of 0.405 nm, as compared with 0.40414 nm for pure Al [25]. The dark-field image in Fig. 3 was obtained from a portion of the {111} ring, as indicated. Selecting different portions of this ring yielded similar images, indicating that the nanocrystallites are randomly oriented. A similar image was reported by Chen et al. [11] without identifying the stress state. The nanocrystallite diameters range from 1.8 to 9.2 nm.

At the fracture surface along the bending axis, which formed as a result of bending, straightening and subsequently, electrolytic thinning, nanocrystallites were also observed. These are shown in a dark-field image in Fig. 4, which also includes the corresponding electron diffraction pattern. The dark-field image in Fig. 4 was also obtained from a portion of the {111} ring, as indicated. The diameters of these nanocrystals are similar to the diameters of those formed at shear bands.

3.2.2. The tensile region

Extensive TEM observations in the tensile region revealed no nanocrystallites at shear bands. Typical bright- and dark-field images are shown in Fig. 5, along with a diffraction pattern. Only diffuse halos are observed in the diffraction pattern, indicating an amorphous phase. The dark-field image was obtained from a portion of the first halo of the diffraction pattern of the amorphous matrix, at the location of the {111} ring observed in the compressive region. It can be seen that the shear bands in this region display a curved morphology, similar to that in the compressive region (Fig. 3). These curved shear bands appear to correspond to the wavy features seen in Fig. 1. Fig. 6 is a dark-field micrograph and corresponding diffraction pattern, of the fracture surface, obtained under conditions similar to those of Fig. 5. Some nanocrystallites are observed, but their density is significantly smaller than that at the fracture surface in the compressive region (Fig. 4). Based on all previous results, we have confidence that these are fcc, Al-rich particles, the volume fraction of which is too small to make a noticeable contribution to the diffraction pattern. This conclusion is supported by the following: (a) an Al-rich fcc phase is the primary product of both thermal and mechanical crystallization [8,11,26]; (b) the {111} diffraction ring is close to the first diffuse ring (inset in Fig. 3) and therefore contributes to the dark-field image even if it is too faint to be visible.

3.3. HRTEM observation

In conventional TEM images, the shear bands appear light and the undeformed region is dark, which is a result of thickness contrast: as they have

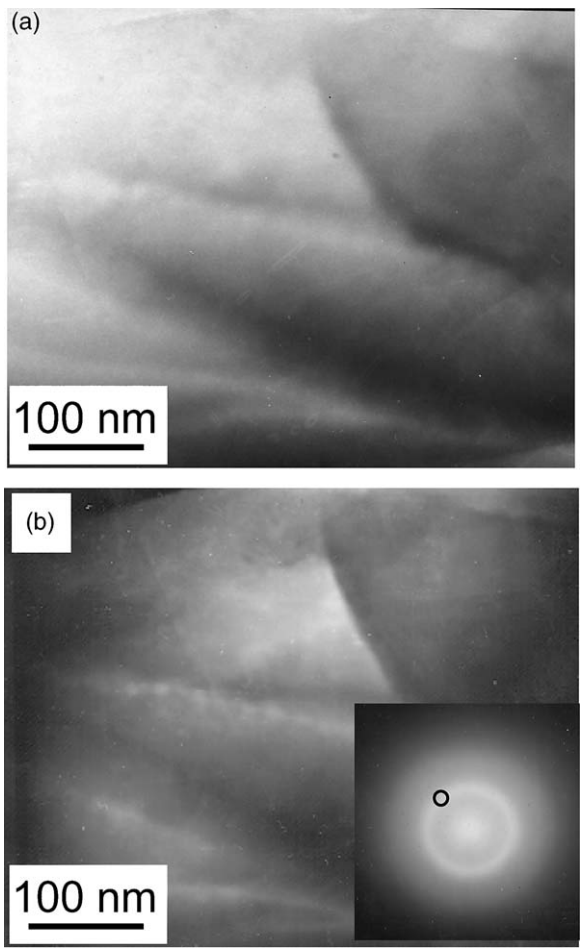

Fig. 5. TEM (a) bright- and (b) dark-field images of the tensile region, showing shear bands. Inset is its SAED pattern, in which the location of the objective aperture is illustrated schematically.

less resistance to chemical attack during thinning, the shear bands are thinned at a higher rate than the matrix [27]. Shear bands were located in HRTEM by continuously increasing magnification of a conventional TEM image centered near the interface between the shear band and undeformed region. Following the method developed by Miller and Gibson [23] and later extended by Li et al. [24], the nanoscale structural characteristics of the shear bands in both the compressive and tensile regions in the bent sample were investigated. It is known that the defocus value in HRTEM is typically set for non-reversed contrast transfer over a

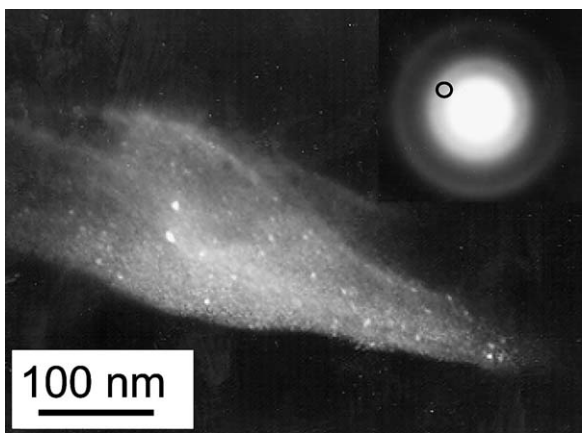

Fig. 6. TEM dark-field image of the fracture surface in the tensile region, established with the first diffraction halo. Inset is its SAED pattern, in which the location of the objective aperture is illustrated schematically.

broad range of wave-vectors. However, such a setting is not ideal for the present work. As detailed below, we detected a prominent difference in the Fourier-transform amplitude between the shear band and undeformed region in the small-angle scattering range, $0.5 < k < 1.5\ \mathrm{nm}^{-1}$. Images were obtained at a defocus value of -200 nm so as to obtain a greater intensity at these values of k, while insuring absence of contrast reversal in the same range [23,24]. For this defocus value, the first zero of the contrast transfer function was calculated to occur at $k = 1.8\ \mathrm{nm}^{-1}$. The Fourier transform of the image was filtered by passing $0.5 < k < 1.5\ \mathrm{nm}^{-1}$ and excluding all other spatial frequencies [24]. The reverse Fourier transform was then calculated to obtain a filtered image, which represents the projected density. The choice of defocus and the filtering are intended to highlight the structural difference between deformed and undeformed regions, and they guarantee the absence of contrast reversal in the filtered image. It is also noted that the filtered image does not display a thickness contrast, since thickness variations are expected to have wave-vectors $k < 0.5\ \mathrm{nm}^{-1}$. Therefore, as seen below, the resulting mesoscopically averaged image intensity is uniform. Regions with locally lower (higher) density appear bright (dark) [24]. To identify density fluctuations, which exceed those expected statistically, a threshold filter was

then applied, set to display a signal only where the mean brightness is exceeded by three standard deviations. Finally, the images were inverted. Although the choice of the threshold filter is somewhat arbitrary and accurate quantification cannot be made, the results are of qualitative, even semi-quantitative significance [23,24].

3.3.1. The compressive region

Fig. 7(a) is a HRTEM image from the compressive region, containing both a shear band and an undeformed region. The shear band appears brighter than the undeformed region. In fact, an image obtained by filtering the Fourier transform to pass only long wavelengths, $k < 0.2$ nm^{-1} (not shown here), confirmed that in Fig. 7(a), the brighter the region, the thinner it is. Recall that there is no contrast reversal for all $k < 1.8$ nm^{-1}. Nanocrystalline particles of about 10 nm diameter are observed within the shear band. Fig. 8(a) is an image filtered as described before, passing $0.5 < k < 1.5$ nm^{-1}. From Fig. 8(a), a threshold-filtered and inverted image was obtained (Fig. 9(a)). In it, the small spots indicate the location of low-density defects in Fig. 7(a). We will refer to these defects, as did Miller and Gibson [23] and Li et al. [24], as nanovoids. There are few nanovoids in the shear band or the undeformed region, and no clear concentration of nanovoids in either region.

3.3.2. The tensile region

Fig. 7(b) displays a HRTEM image from the tensile region, containing both a shear band and an undeformed region. Again, the shear band appears bright and the undeformed region dark, but no nanocrystals are observed. Using the same parameters as for the compressive region, a frequency-filtered image (Fig. 8(b)) and, subsequently a threshold-filtered, inverted, image (Fig. 9(b)) were obtained. The shear band is observed to contain a uniform distribution of nanovoids, the density of which is higher than that in the undeformed region. This is substantially different from our observation in the compressive region (Fig. 9(a)).

Comparing the results for the compressive region with those for the tensile region, it is evident that features viewed by this technique results from the structural details of the materials, rather than from a thickness effect. This comparison also lends support to the effectiveness of the method. It should be cautioned that a comparison of the absolute densities of defects in Fig. 9(a) and (b) is not possible. Despite the fact that the images were processed in the same way, the imaging conditions for Fig. 9(a) and (b) were not identical, resulting in

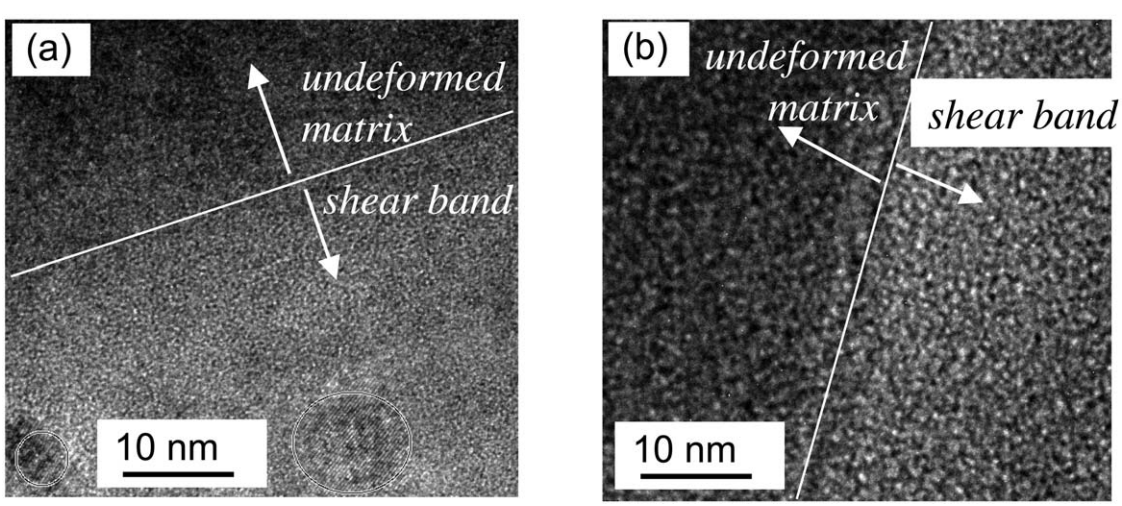

Fig. 7. HRTEM images of a shear band (bright) and an undeformed matrix (dark) in the (a) compressive and (b) tensile regions. The lines drawn indicate the boundary between the shear band and the undeformed matrix.

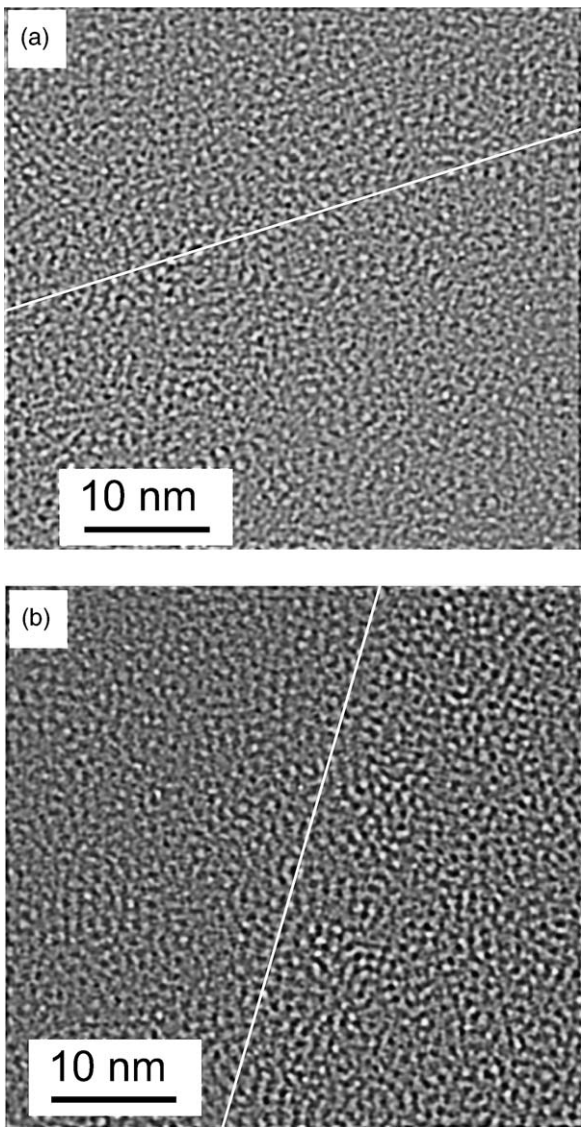

Fig. 8. (a,b) Images corresponding to Fig. 7(a) and (b), respectively, but defocused −200 nm, Fourier filtered. The lines drawn indicate the boundary between the shear band and the undeformed matrix.

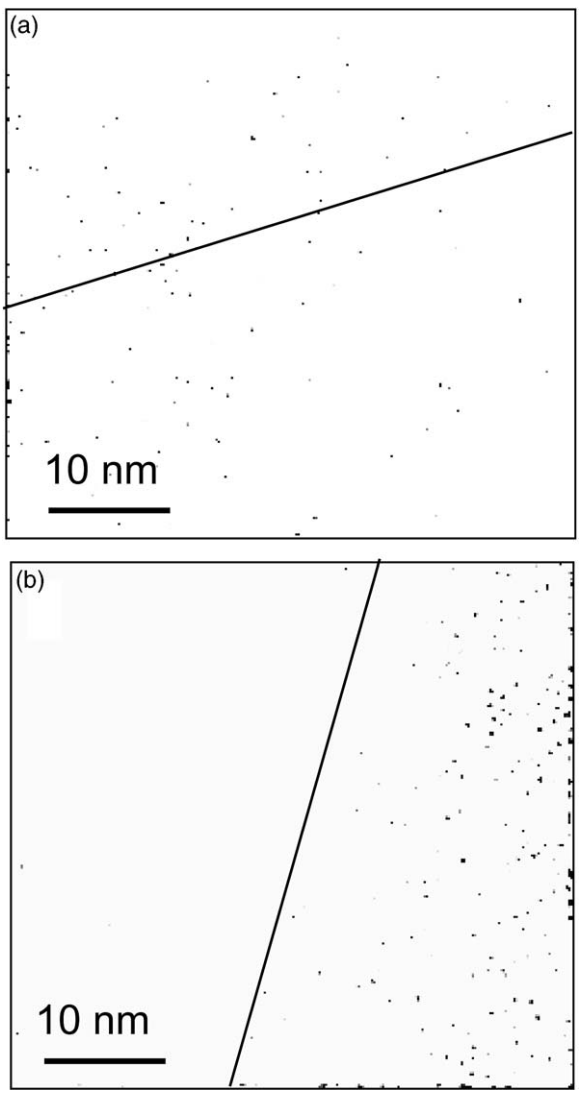

Fig. 9. (a,b) Images corresponding to Fig. 8(a) and (b), respectively, but threshold filtered and inverted. The lines drawn indicate the boundary between the shear band and the undeformed matrix.

an incomparability in the intensity. Although the threshold filters were set using the same criterion, the standard deviation is larger for the image of the tensile region, in which the density fluctuations at the shear band are larger. It is the comparison of variations within each sample that is significant.

4. Discussion

In addition to the long-exposure experiment in the TEM, the fact that nanocrystallites were only observed in some regions of some of the samples, and not in the as-spun sample, further supports our assertion that the crystallites did not form as a result of electron-beam-induced heating or ballistic

displacements in the TEM. Similarly, in addition to X-ray diffraction in cold-rolled samples, the present results confirm that the observed nanocrystallites were not created during TEM sample preparation. Most significantly, even in the presence of shear bands, only the compressive region contained nanocrystallites. Indeed, the formation of nanocrystallites induced by mechanical deformation is typically observed under compressive stress, such as obtained by ball milling [8], rolling [13], or indentation [16]. While Chen et al. [11] did not identify the sign of the stress, we suggest that their observations were made in predominantly compressive regions, as their material and deformation condition are the same as ours. Inoue et al. [28] reported the formation of nanoscale Al particles during tensile deformation at elevated temperature in amorphous $Al_{88}Ni_{10}Ce_2$. However, their tensile tests were conducted at temperatures sufficiently high to cause purely thermal crystallization. Gao et al. [14] observed the precipitation of nanocrystallites in amorphous $Al_{90}Fe_5Gd_5$ subjected to tensile test at room temperature, but only at the fracture surface. We are not aware of reports of crystallization at shear bands formed by tension.

At room temperature, amorphous alloys exhibit extremely low ductility during uniaxial tension, and develop few shear bands up to catastrophic failure. This makes it difficult to identify the structural features of the shear bands. Bending, on the other hand, can produce a number of shear bands around the bending axis in both the tensile and compressive regions. While it creates complicated stress states, bending provides a feasible route to study the effects of compression and tension on shear bands and nanocrystallization.

The task of identifying the mechanisms of nanocrystallization induced by mechanical deformation is challenging. As described before, a temperature spike has been suggested, based on composition profiles at precipitates [22] and melting at fracture surfaces [14]. Assuming adiabatic heating, Chen et al. [11] estimated a temperature increase as high as 2500 K at shear bands of Al-based amorphous alloys. They also argued that heat dissipation by conduction would take place on a nanosecond timescale, thus bypassing crystallization. If a temperature spike were the cause of crystallization, one would expect all alloys in this family to undergo mechanical crystallization, since they have similar crystallization temperatures and mechanical behavior. However, bending and ball milling experiments showed that the formation of nanocrystallites is sensitive to the alloy compositions. Bending failed to induce precipitation of nanocrystalline Al particles in $Al_{85}Ni_{10}Ce_5$ alloy [11]. Also, ball milling for 5 h could not cause the formation of nanocrystallites in amorphous $Al_{85}Ni_5Y_{10}$ [8]. Furthermore, the present work shows that only the shear bands in the compressive region are preferential sites for formation of nanocrystallites and those in the tensile region are not. Since a similar temperature increase is expected in compression or tension, these results strongly support the notion that local heating is not the cause of crystallization.

We believe the present work to be the first to show that mechanically induced nanocrystallization of Al-based amorphous alloys at shear bands occurs only in the compressive region. Undoubtedly, this phenomenon is best explored by studying the structural nature of the shear bands. Unlike in crystalline alloys, the direct observation of defects in amorphous alloys is challenging. Using a recently developed quantitative HRTEM technique, the present work clearly demonstrates a substantial difference between shear bands in the tensile and compressive regions. In the tensile region, shear bands contain a higher density of nanovoids than the surrounding undeformed region (Fig. 9(b)). In the compressive region, there are few nanovoids, and they are not confined to one region. Li et al. [24], using the same method for a Zr-based amorphous alloy, reported a higher density of nanovoids in shear bands than in the amorphous matrix. The shear bands were at the tip of cracks developed during the sample's electropolishing. The nature of the stress state under which they formed is unknown. In an investigation of shear bands in deformed, amorphous, nickel-phosphorus thin films, using an axially aligned dark-field technique of TEM, Donovan and Stobbs [29] observed dilated bands forming in both compression and tension. They also observed a large small-angle scattering signal for shear bands obtained in tension, which they attributed to voids. They argued that

the shear bands were dilated in both compression and tension, which is required for atomic motion to take place, but that compressive stress prevented the formation of voids. These results are analogous to ours. Li et al. [30] and Wright et al. [31] have analyzed the thermodynamics of coalescence of excess free volume into voids. It would be instructive to expand the analysis to include the effect of stress.

Amorphous alloys are known to have a varying amount of excess free volume. Regions with high free volume are expected to have a lower strength. Steif et al. [32] and Argon [33], in their free volume creation models, suggested that a pre-existing narrow "weakened band" precedes the localization of plastic flow. The weakened band may develop into a highly localized deformed band, i.e. shear band, during mechanical deformation. The shear strain within the shear band can be as high as 10^2–10^3% in a bent sample [11]. Therefore, a large proportion of the atoms within shear bands are subject to local displacements. Thus, atomic dilatation in the shear bands is the likely cause of enhanced atomic mobility. However, the condensation of free volume into nanovoids in the tensile region reduces its availability to enhance the atomic diffusion rate.

We finally note that there is also a potential contribution of the stress to the driving force. Ye and Lu [17] reported that hydrostatic stress increased the driving force for crystallization in a similar alloy. In the compressive (tensile) region, there is likely to be a hydrostatic compressive (tensile) stress in the shear bands, enhancing (reducing) the driving force for crystallization. Our observations on the effect of strain rate on the size and density of nanocrystallites [16] show that the effect of hydrostatic stress on the driving force cannot, by itself, account for the nanocrystallization.

In the present work, some nanocrystallites were observed at the fracture surface along the bending axis in the tensile region (Fig. 6). Under SEM, we observed that cracks formed after bending and straightening along the bending axis at both the compressive and tensile sides, where the most severe deformation occurred. Cracks possibly propagated during subsequent electrolytic thinning. The formation of nanocrystallites at cracks is a likely result of adiabatic heating during fracture, as concluded by Gao et al. [14]. Wright et al. [34] also observed localized melting at the fracture surface of bulk amorphous $Pd_{40}Ni_{40}P_{20}$ obtained in uniaxial compression, indicating that adiabatic heating occurred during the final failure. Low strain rates were employed in both Refs. [14,34].

We conclude from the difference in crystallization at shear bands in compression versus tension that the effect of the adiabatic heating on nanocrystallization at shear bands is much less significant than enhancement of atomic mobility by deformation. On the other hand, at fracture surfaces, since crystallization is observed in both compression and tension, and considering Refs. [14,34], adiabatic heating is a likely significant contributor to crystallization. The higher density of nanocrystallites at the fracture surface in the compressive region, as compared with that at the fracture surface in the tensile region, may be due to an additional contribution of atomic-mobility enhancement by deformation prior to fracture.

5. Summary

Using TEM and HRTEM techniques, the effect of bending at room temperature on the microstructure of amorphous $Al_{90}Fe_5Gd_5$ was investigated in detail. The main results can be summarized as follows.

1. In the compressive region, nanocrystallites formed preferentially at shear bands, along small cracks and at the fracture surface. In the tensile region, nanocrystallites were observed only at the fracture surface.
2. Combining HRTEM with Fourier transform and filtering techniques, nanovoids were imaged. In the compressive region, both the shear bands and the undeformed matrix contain few nanovoids. In the tensile region, the shear bands contain more nanovoids than the surrounding, undeformed, matrix.
3. The preferential precipitation of nanocrystallites in the compressive region is attributed to a kinetic effect due to the uniformly distributed free volume in the shear bands. A contribution of

hydrostatic stress to the driving force is possible, but not dominant.

4. The formation of nanocrystallites at the fracture surfaces in both the compressive and tensile regions is likely caused by adiabatic heating, induced by fracture produced by bending, straightening as well as subsequent electrolytic thinning.

Acknowledgements

The authors acknowledge useful discussions with Prof. F. Spaepen (Harvard University). They are also grateful to Dr F.E. Pinkerton (General Motors Research Laboratories) for providing the samples used in this study. The electron microscopy work was performed at the Electron Microbeam Analysis Laboratory at the University of Michigan. This work was funded by the US National Science Foundation, grant DMR-9902435.

References

[1] Shiflet GJ, He Y, Poon SJ. Scr Metall 1988;22:1661.
[2] He Y, Poon SJ, Shiflet GJ. Scr Metall 1988;22:1813.
[3] Chen H, He Y, Shiflet GJ, Poon SJ. Scr Metall Mater 1991;25:1421.
[4] Kim YH, Choi GS, Kim IG, Inoue A. Mater Trans JIM 1996;37:1471.
[5] Sun WS, Quan MX. Mater Lett 1996;27:101.
[6] Kulik T. J Non-Cryst Solids 2001;287:145.
[7] Lu K. Mater Sci Eng R 1996;16:161.
[8] He Y, Shiflet GJ, Poon SJ. Acta Metall Mater 1995;43:83.
[9] Fan GJ, Quan MX, Hu ZQ, Löser W, Eckert J. J Mater Res 1999;14:3765.
[10] Xu J, Atzmon M. Appl Phys Lett 1998;73:1085.
[11] Chen H, He Y, Shiflet GJ, Poon SJ. Nature 1994;367:541.
[12] Ogura A, Sato M, Tarumi R, Shimojo M, Takashima K, Higo Y. Mater Res Soc Symp Proc 2001;634:B1.
[13] Jin HJ, Zhou F, Wang LB, Lu K. Scr Mater 2001;44:1083.
[14] Gao MC, Hackenberg RE, Shiflet GJ. Mater Trans JIM 2001;42:1741.
[15] Kim JJ, Choi Y, Suresh S, Argon AS. Science 2002;295:654.
[16] Jiang WH, Pinkerton FE, Atzmon M. J Appl Phys 2003;93:in press.
[17] Ye F, Lu K. Acta mater 1999;47:2449.
[18] Zhuang YX, Jiang JZ, Zhou TJ, Rasmussen H, Gerward L. Appl Phys Lett 2000;77:4133.
[19] Johnson WL. Prog Mater Sci 1986;30:81.
[20] Johnson WL. In: Westbrook JH, Fleischer RL, editors. Intermetallic compounds, vol. 1. Chichester, England: Wiley; 1994. p. 700.
[21] Xu J, Collins GS, Peng LSJ, Atzmon M. Acta mater 1999;47:1241.
[22] Csontos AA, Shiflet GJ. Scr Mater 1997;9:281.
[23] Miller PD, Gibson MJ. Ultramicroscopy 1998;74:221.
[24] Li J, Wang ZL, Hufnagel TC. Phys Rev B 2002;65:144–201.
[25] Pearson WB. In: A handbook of lattice spacing and structures of metals and alloys. London: Pergamon Press; 1958. p. 124.
[26] He Y, Chen H, Shiflet GJ, Poon SJ. Philos Mag Lett 1990;61:297.
[27] Pampillo CA. Scr Metall 1972;6:915.
[28] Inoue A, Kim YH, Masumoto T. Mater Trans JIM 1992;33:487.
[29] Donovan PE, Stobbs WM. Acta Metall 1981;29:1419.
[30] Li J, Spaepen F, Hufnagel TC. Philos Mag 2002;82:2623.
[31] Wright WJ, Hufnagel TC, Nix WD. J Appl Phys 2003;93:1432.
[32] Steif PS, Spaepen F, Hutchinson JW. Acta Metall 1982;30:447.
[33] Argon AS. Acta Metall 1979;27:47.
[34] Wright WJ, Schwarz RB, Nix WD. Mater Sci Eng A 2001;319/321:229.